JOURNAL OF CATALYSIS 102, 419–432 (1986)

Interpretation of Hydrogen Chemisorption on Nickel Catalysts

JAMES T. RICHARDSON* AND TIMOTHY S. CALE†

*Department of Chemical Engineering, University of Houston, University Park, Houston, Texas 77004; †Department of Chemical and Bioengineering, Arizona State University, Tempe, Arizona 85281

Received December 31, 1984; revised August 5, 1986

The origin of reversible hydrogen adsorption on dispersed nickel catalysts has been examined through analysis of *in situ* magnetization and chemisorption measurements on a large number of silica- and alumina-supported catalysts. Parameters considered were crystallite size, extent of reduction, calculated surface capacity, N_M, measured surface capacity for irreversible adsorption, N_0, slope of the reversible isotherm, b, and surface accessibility, N_0/N_M. Relationships between experimental variables were used to rule out certain models explaining reversible adsorption and to support others. Adsorption on the support, spillover, reaction with unreduced nickel compounds, and surface contamination were eliminated from considerations as inconsistent with observed magnetic responses. Site heterogeneity within the monolayer was considered unlikely from temperature dependence and other factors. The most significant effect was a correlation between the degree of accessibility and the areal slope b/N_0 showing that the amount of reversible adsorption increased as surface accessibility decreased. This minimized consideration of multilayer adsorption on subsurface sites and diffusion into the bulk of the crystallite but reenforced the concept of diffusion into the inaccessible region of the surface. Extrapolation of hydrogen adsorption isotherms to zero pressure is recommended as the best method for measuring exposed surface.

INTRODUCTION

Hydrogen has become a preferred adsorbate for characterizing metal surface areas with chemisorption isotherms (*1*). Other gases, such as carbon monoxide (*2*), oxygen (*3*), and hydrogen sulfide (*4*) are uncertain because of imprecise knowledge of adsorption stoichiometries or penetration into deeper surface layers. Supported noble metals readily form distinct monolayers and hydrogen chemisorption gives metal surface areas in good agreement with other techniques (*5*). However, interpretation is far from clear in the case of supported nickel. The purpose of this paper is to examine alternative adsorption models in order to clarify the situation.

Figure 1 illustrates typical isotherms from volumetric adsorption techniques. Initially there is a rapid adsorption at low pressures. Using small hydrogen pulses in a Pulsed Thermokinetic (PTK) study, Richardson and Friedrich showed that this adsorption is irreversible and desorbs very slowly (*6*). Saturation is reached with an average heat of adsorption of 20 kcal/mole.

Irreversible adsorption is followed by a much slower uptake, approximately linear with pressure. Apparent equilibrium is slowly attained over a peiod of minutes or hours. There is always some uncertainty since slow adsorption continues up to a point where the integrity of the vacuum system forces the operator to declare steady state. This mode of adsorption is reversible and evacuation rapidly removes it. Readsorption follows a linear path parallel to the original isotherm but separated from it by an amount equal to the irreversible mode.

Data in Fig. 1 are representative of a large number of experiments in which hydrogen chemisorption and magnetic measurements were performed on the same sample. Details are given elsewhere (*7–10*). This procedure allows comparison of the amount of hydrogen adsorption, N_A, as measured from hydrogen adsorption, with a value calculated from magnetically derived

0021-9517/86 $3.00

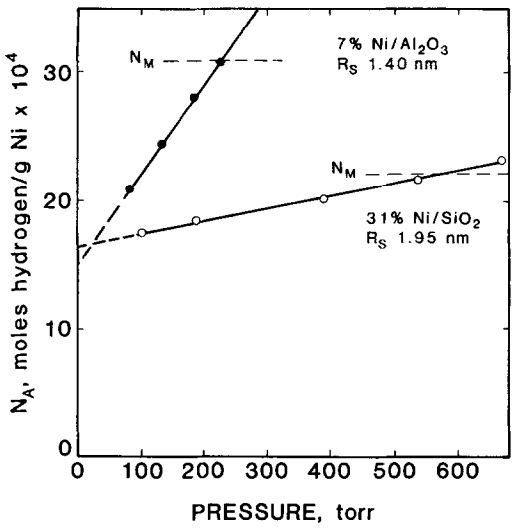

FIG. 1. Typical hydrogen chemisorption isotherms on supported nickel.

crystallite size distributions, N_M. The magnetic method, perfected over many years of use, provides magnetization versus magnetic field curves from which several useful parameters are extracted. First, the saturation magnetization, M_∞, is a direct measure of the amount of reduced nickel, giving the fraction reducibility, f_R. Secondly, the shape may be used to calculate crystallite volume size distributions, from which the number of surface sites, N_M, are deduced if spherical shapes are assumed. For other shapes, N_M varies accordingly but not significantly. The following are apparent in Fig. 1: (1) Irreversible adsorption is less than full monolayer coverage indicated by N_M. (2) Reversible adsorption does not saturate at experimental pressures. (3) There are differences in the slopes of the isotherm for different samples.

These results agree with measurements reported by others, although some find saturated isotherms for conditions giving complete reduction (*11*). Deciding on monolayer coverage becomes somewhat arbitrary. Some authors extrapolate the isotherm to zero pressure (*12*), others select specific pressures such as 100, 300, or 760 Torr (*13–15*). In some cases, the Langmuir isotherm is found to fit (*16*). Recently the Freundlich isotherm was used (*17*).

In the absence of saturation there is no justification for any of these procedures. Only an understanding of the nature of the reversible adsorption will lead to the correct method. We list most of the proposed rationalizations below, together with a brief description. More detailed arguments follow later.

(*1*) *Adsorption on the support.* Support materials such as SiO_2 and Al_2O_3, with impurity levels of transition oxides, may have weak adsorption sites for hydrogen, especially when reduced. Although parallel measurements on supports usually reveal negligible adsorption, this explanation cannot be completely dismissed since preparational procedures for nickel deposition may develop adsorption sites on the support.

(*2*) *Spillover onto the support.* A more sophisticated version of support adsorption, this explanation is valid especially in view of the large amount of evidence supporting spillover phenomena (*18, 19*). During spillover, adsorption generates hydrogen atoms on nickel followed by diffusion to the support and subsequent replacement of hydrogen on the nickel surface. Since extent of hydration of the surface is a factor, support type and pretreatment are important parameters.

(*3*) *Adsorption on unreduced nickel compounds.* Supported nickel catalysts as usually prepared consist of a variety of nickel compounds before reduction—salts, hydroxides, oxides, aluminates, silicates, etc. These are often difficult to reduce so that the catalyst is a mixture of nickel metal and unreduced precursor. The latter could adsorb hydrogen weakly and reversibly (*20*).

(*4*) *Reaction with surface contamination.* Highly dispersed nickel is very reactive with oxygen. During experimental operations, nickel could become partially covered with patches of adsorbed oxygen or even an oxide film. Oxygen can originate from impurities in inert gases used to clean

the catalyst or from leaks during prolonged evacuation. Another source is the support itself, especially after extensive heating in the absence of hydrogen. Hydrogen reacts with chemisorbed oxygen and replaces the Ni—O bond with Ni—H. Selwood determined oxygen–nickel stoichemistry to be 1:2 for low partial pressures of oxygen (*21*), so that the reaction is

$$Ni_2—O + 2H_2 = H_2O + 2\ Ni—H \quad (1)$$

This is similar to the oxygen titration method sometimes used to measure surface areas (*22*).

Other contaminants, such as carbon, could act in a similar manner.

(*5*) *Heterogeneous sites.* Possibility of adsorption site heterogeneity is very real. Crystallographic and experimental evidence strongly suggests that a wide spectrum of modes and energetics of adsorption exists (*23*). Hardeveld and Hartog proposed that the statistics of these sites may be represented with an imperfect cubooctahedron model for nearly spherical crystallites (*24*). Principal crystallographic planes are (100), (110), and (111). Further site discrimination is possible with face, edge, and corner atoms on these planes. Steps and kinks add further complexity (*25*). Bond extended the concept by including orbital symmetry considerations, leading to many different modes of adsorption (*26*). Although supported by early calculations of Shopov *et al.* (*27*), this model has since been challenged by Fassaert and van der Avoird (*28*). Nevertheless, evidence for site heterogeneity persists. Sweet and Rideal reported very strong adsorption at coverages from zero to 0.1 with heats of adsorption from 32 to 25 kcal/mole (*29*). This is in agreement with earlier measurements and is assigned by Sweet and Rideal to adsorption on corners and edges. Calculations by Fassaert and van der Avoird agree but further indicate that adsorption on (100), (110), and (111) planes occurs preferentially on top of nickel atoms with very little plane specificity in heats of adsorption (*30*). Christmann (*31*) and Lapeyoulade and Neil (*32*) found about 22 kcal/mole decreasing to 14 kcal/mole above a coverage of 0.5. Sites with multiple bonding and "hole" positions in the layer one-half of an atomic distance below the surface are estimated to have heats below this range. Slinken *et al.* found a correlation between irreversible adsorption and the ratio of corner and edge sites assuming rhombic dodecahedra, but with limited samples (*33*).

Sites with medium to very strong adsorption heats (20 to 35 kcal/mole) could account for irreversible adsorption and follow Langmuir isotherms with large adsorption coefficients. Multiple bonding and "hole" adsorption result in weakly held hydrogen (i.e., reversible) with correspondingly small coefficients.

The overall isotherm is

$$N_A = \sum_{\substack{i \\ \text{strong}}} \frac{N_{I,i} K_{I,i}^{1/2} P_H^{1/2}}{1 + K_{I,i}^{1/2} P_H^{1/2}} + \sum_{\substack{j \\ \text{weak}}} \frac{N_{R,j} K_{R,j}^{1/2} P_H^{1/2}}{1 + K_{R,j}^{1/2} P_H^{1/2}} \quad (2)$$

where

$N_{I,i}$ = saturation coverage of i strong sites with adsorption coefficient $K_{I,i}$

$N_{R,j}$ = saturation coverage of j weak sites with adsorption coefficient $K_{R,j}$

P_H = hydrogen pressure.

For $K_{I,i}^{1/2} P_H^{1/2} \gg 1$ and $K_{R,j} P_H^{1/2} \ll 1$ Eq. (2) reduces to

$$N_A = N_0 + b P_H^{1/2} \quad (3)$$

where

$$N_0 = \sum_i N_{I,i}$$

and

$$b = \sum_j N_{R,i} K_{R,j}^{1/2}.$$

Equation (3) has the same general shape as the isotherms in Fig. 1 over a limited pressure range.

(*6*) *Multilayer adsorption.* Adsorption on corner, edge, and top positions of the low index planes would normally be defined as a monolayer. Penetration into the second layer (i.e., bridge and "hole" positions) is an excess of the monolayer. This view is supported by Konvalinka *et al.* who found at least seven adsorption modes with temperature programmed desorption (TPD) (*34*). These authors, however, consider reversible low heat, modes to be "type C" chemisorption, discussed generally by Bond (*35*). Pictured as a predissociative, species formed from combinations of other modes, they are limited to only a fraction of a monolayer. It is possible that much of the reversible adsorption shown in static isotherms was not observed during the TPD studies due to experimental procedures.

(*7*) *Surface inaccessibility.* Richardson and Desai discussed "surface inaccessibility" occurring when measured surface areas are less than those calculated from size determinations (*8*). Presumably part of the surface is inaccessible to hydrogen. Whether this is due to a "skin" of support over the metal, as first suggested by Linsen and Coenen (*36*), to pore trapping (*37*) or to strong metal–support interactions (SMSI) (*38–40*) is not obvious. Irreversible adsorption could be a measure of exposed or accessible surface. Reversible uptake could follow diffusion from this surface into the "skin" or otherwise inaccessible surface. The mechanism is not clear, but to a first approximation isotherms similar to Eq. (3) may be derived, with the exception that the coefficient b is not an equilibrium coefficient but a kinetic factor. Exact values depend on experimental conditions.

(*8*) *Bulk diffusion.* Permeation of hydrogen into metal surfaces is a well-known phenomena and has been reviewed by McLellan and Harkins (*41*). Extensive research has shown that hydrogen does indeed absorb in nickel with formation of Ni—H bonds and loss of magnetization. Measured permeation rates in bulk metal are, however, exceedingly small (*41*). Selwood concluded that absorption is not a reasonable explanation for reversible uptake (*21*). However, Messmer *et al.* calculated that the electronegativity difference between hydrogen and nickel decreases as the crystallite becomes small, leading to much larger permeation rates for highly dispersed catalysts (*42*). In some cases, as much as 4–5 times monolayer coverage has been detected with platinum (*43*).

(*9*) *Strong metal–support interaction.* Easily reducible supports, such as TiO_2, affect the adsorption properties of dispersed metals (*38*). Following reduction at high temperatures, ability to adsorb hydrogen is drastically decreased. More common supports, SiO_2 and Al_2O_3, show similar but less dramatic effects (*40*). Whether due to electron transfer (*38*), activated hydrogen adsorption (*44*) or surface alloy formation (*45*), the phenomenon could be related to generation of sites for reversible adsorption.

Many of these mechanisms were covered in a review by Knor (*46*) but the question of the nature of the reversible mode was not considered.

In view of the many alternatives it is not surprising that no consensus exists for interpreting hydrogen isotherms. However, some may be eliminated by considering two critical properties.

The first is the magnetization loss upon hydrogen chemisorption. Selwood was the first to address this problem using both low and high field measurements (*21*). The effect has been confirmed since then (*47*). Saturation magnetization of a surface nickel atom decreases by 0.73 Bohr magnetons upon chemisorption of one hydrogen atom. This is interpreted as electron donation to the *d*-band in nickel, effectively filling the 0.606 *d*-holes responsible for magnetization and influencing neighboring atoms by decreasing magnetic interaction. Dissociation is implied. The magnetization decrease (ε) is the same for both irreversible and reversible adsorption, indicating that, although the strength of adsorption is dif-

ferent, dissociation and nickel interaction is the same. Selwood found the effect to persist up to pressures of hundreds of atmospheres, concluding that "full coverage is never reached." Desorption reverses the process. These observations rule out support adsorption, adsorption on unreduced nickel and predissociative type-C adsorption as major contributors to reversible uptake.

The second feature is the actual reversibility itself. Surface contamination becomes questionable. Reversibility, together with regain of magnetization, is not likely to occur in the case of spillover.

Possibilities now begin to narrow. Presumably strong adsorption (20 kcal/mole or greater) at low pressure could be monolayer coverage of corner, edge, and low index sites of the accessible surface. Further uptake occurs through diffusion away from these sites to less accessible, lower energy positions with replacement of the original adatom. Diffusion could be either to subsurface positions just below the exposed atoms, into the bulk of the crystallite, or to the inaccessible portion of the surface nickel, between the crystallite and support.

The implication is that exposed surface is best measured by extrapolation to zero pressure using Eq. (3). The conclusion is correct only if the diffusion processes in (1), (2), or (3) above are confirmed, a difficult task. Much of existing evidence has been obtained by different researchers, using widely varying experimental techniques on samples prepared in many ways. Results are inconsistent and no trends obvious.

However, techniques have been developed in this laboratory for measurement of hydrogen isotherms, crystallite size distribution and degree of reduction on the same sample (*9*). Uncertainties introduced by experimental methods inherent in different sampling techniques are avoided and more reliable information obtained.

Several such studies have been made over the past 5 years, involving different investigators studying similar catalysts under a wide range of conditions (*48–50*). From this information it is possible to extract consistent themes that confirm the appropriateness of an interpretation, as well as shedding further light on the complex nature of reversible hydrogen adsorption.

EXPERIMENTAL

Catalyst preparation. Homogeneous precipitation–deposition techniques were used to prepare two types of catalysts reported in this work (*51*). The supports were (1) SiO_2 in the form of Cab-O-Sil and (2) samples of γ-Al_2O_3 of differing pore size distributions (*50*). Each support was slurried with nickel nitrate solution and urea at 90°C. Slow hydrolysis of urea produced a very homogeneous and highly dispersed nickel compound precipitated on the support.

Final products ranged from 20 to 35 wt% Ni on SiO_2 and 5 to 10 wt% Ni on Al_2O_3.

Reduction procedures. Samples were loaded into *in situ* cells described in detail earlier (*9*), reduced in hydrogen at 350–500°C, and cleaned in He at slightly higher temperatures. Magnetic and chemisorption measurements were then carried out as reported. Saturation magnetization values for samples cleaned at different temperatures were identical, indicating that this procedure does indeed remove adsorbed hydrogen without surface-induced oxidation (*9, 37, 51*).

Magnetic measurements. Magnetization measurements covered the range 0 to 15 kOe and −196 to 25°C and data used to estimate the fraction of nickel reduced, f_R, crystallite size distribution, calculated surface area, S_M, m^2/g Ni(red), and surface monolayer capacity N_M, moles H_2/g Ni(red). Exact procedures are described in earlier publications (*9*).

An improved apparatus was used in some of the experiments, involving a Vibrating Sample Magnetometer manufactured by Princeton Applied Laboratories and a Varian electromagnetic, together with a specially designed quartz cell for *in situ* mea-

TABLE 1

Statistics of Nickel Parameters

Catalyst: 32 wt% Ni/SiO_2 Reduction: 400°C, 6 h					
Run No.	f_R	R_s (nm)	$N_0 \times 10^4$	$b \times 10^4$	b/N_0
1	0.735	1.33	11.3	0.293	.0259
2	0.707	1.16	11.3	0.313	.0277
3	0.732	1.19	10.3	0.267	.0259
4	0.709	1.33	11.3	0.282	.0250
Average	0.721	1.25	11.0	0.288	.0261
SD	0.015	0.09	0.5	0.019	.0011

Note. f_R, fraction of nickel reduced; R_s, average crystallite radius based on surface area calculated from magnetic crystallite size distribution; N_0, intercept of Eq. (3), moles H_2/g Ni(red); b, slope of Eq. (3), moles of H_2/g Ni(red) · Torr.

surements (*48*). This equipment measured the rate of magnetization loss upon hydrogen adsorption, leading to rates of hydrogen chemisorption at constant pressure.

Chemisorption measurements. Volumetric chemisorption studies were made directly on the same sample in the magnetometer cell using an apparatus reported previously (*9*). Reduction and cleaning procedures were the same but the sample was evacuated for several hours at the cleaning temperature. Sufficient time (5–45 min) was allowed for equilibrium or pseudoequilibrium in each point. This gave the isotherm at 25°C in terms of N_A, moles H_2/g Ni(red), versus hydrogen pressure. Typical results are given in Table 1, using Eq. (3) to determine N_0 and b.

Experimental conditions. The results discussed in this work were obtained over a 5-year period on different studies of crystallite size effects in catalysis. Many of these experiments are described elsewhere (*7–9, 37, 48–50*). Sample preparation and measurement techniques were the same. Six different operators were involved in these studies. Some degree of reproducibility is seen in data shown in Table 1. These were identical measurements on four different samples of the same catalyst. Runs 1, 2, and 3 were carried out by one operator, Run No. 4 by another. This level of precision has been achieved repeatedly. Statistical parameters in Table 1 are used to reach certain conclusions regarding significance of experimental variations. They reflect the precision of both the magnetic (f_R and R_s) and the chemisorption (N_0 and b) parameters.

RESULTS AND DISCUSSION

Shape of the Isotherm

Most of the hydrogen chemisorption data were taken in the pressure range 25 to 300 Torr. The isotherm shown in Fig. 2 was obtained with measurements extended to lower pressures. The sample was 32 wt% Ni/SiO_2 reduced at 400°C. Magnetic characterization gave an average "surface" radius, R_s, of 1.35 nm, with a fraction of reduced nickel, f_R, of 0.709. For low pressure points (<10 Torr) adsorption was rapid and equilibrium reached in minutes. Much longer times were required for higher pressure readings. Usually 45 min to 1 h were sufficient. At this "steady state," true equilibrium was not established but further changes were very slow.

The data in Fig. 2 were fitted to a modification of Eq. (2)

$$N_A = \frac{N_I K_I^{1/2} P_H^{1/2}}{1 + K_I^{1/2} P_H^{1/2}} + N_R K_R^{1/2} P_H^{1/2} \quad (4)$$

with a regression coefficient of 0.9976. The isotherm shape is generally consistent with the model of Langmuir-type, dissociative adsorption on a very strong site followed by adsorption on weaker sites. At higher pressures, Eq. (4) reduces to Eq. (3), which was used to analyze all subsequent data. Significantly better statistical precision was achieved compared to first-order pressure dependence. However, the exact significance of b, whether thermodynamic or kinetic, depends upon the prevailing mechanism.

Heats of Adsorption

A sample of 20 wt% Ni/SiO_2 (f_R = 0.95, R_s = 1.74 nm) was studied over a wide pres-

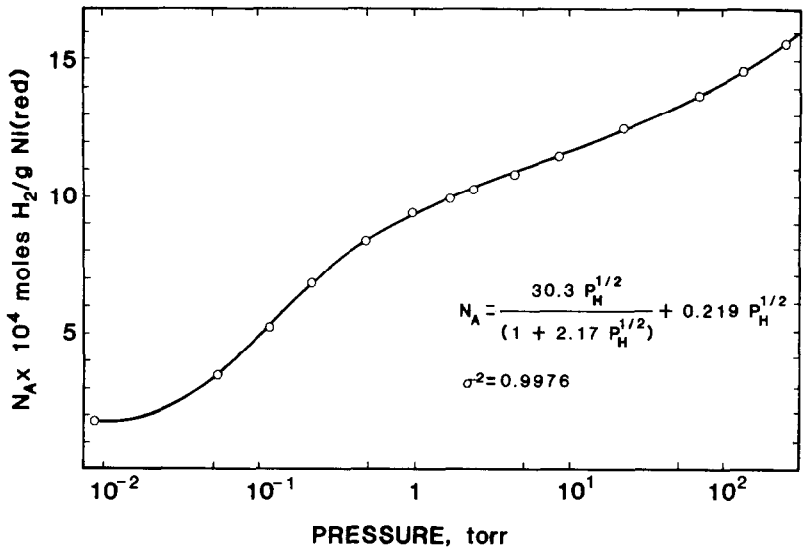

FIG. 2. Pressure dependence of hydrogen chemisorption.

sure range at 30 and 40°C and isosteric heats of adsorption calculated from the isotherm. Results are superimposed on the 30°C isotherm shown in Fig. 3, indicating an almost constant value of 18–19 kcal/mole for irreversible adsorption with an immediate decrease at the onset of reversible adsorption. This decrease continues with coverage. Interpretation of isoteric heats of adsorption in this manner may not be completely justified, yet results are remarkably consistent with previous determinations.

Whether or not the decrease is due to heterogeneity in adsorption sites or to induced effects from repulsion of adatoms is not clear from these measurements alone.

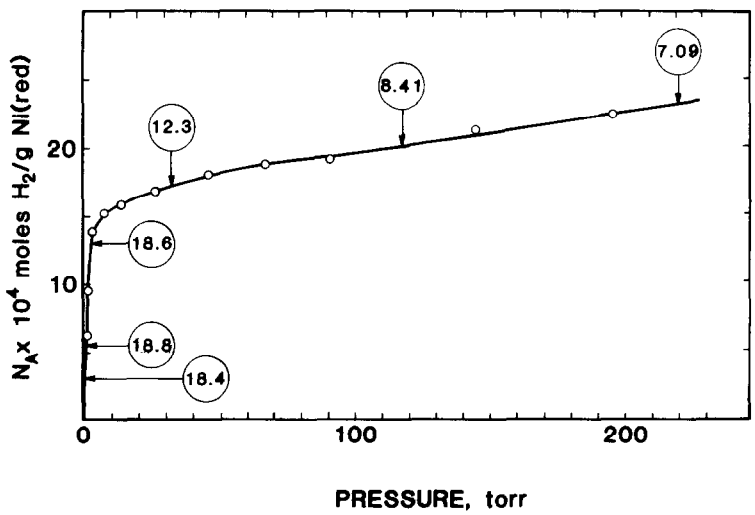

FIG. 3. Temperature dependence and heats of adsorption of hydrogen chemisorption.

TABLE 2

Effect of Temperature on Adsorption Parameters

	Sample: 20% Ni/SiO_2 Reduction: 400°C, 16 h R_s: 1.74 nm f_R: 0.95	
T (°C)	$N_0 \times 10^4$ moles/g Ni(red)	$b \times 10^4$
23	15.7	0.273
30	16.2	0.273
39	16.4	0.287
51	15.4	0.288
60	14.4	0.290
70	12.1	0.371
80	11.4	0.409
100	10.2	0.415

Temperature Effects

Measurements were extended to higher temperatures for the sample in Fig. 3. Table 2 shows the parameters found for Eq. (3).

Initially, both N_0 and b remain essentially constant. Above about 50°C, N_0 decreases and b increases. The multiple site model implies that b should decrease due to temperature dependence of K_R. However, with increasing temperature weaker irreversible sites become more reversible, decreasing N_0 and increasing b through N_R.

Alternatively, if b reflects kinetic rather than equilibrium effects, then b should increase with temperature.

Rate of Adsorption

Magnetization loss was used to measure rates of adsorption. In order to confirm that magnetization loss is identical for different modes of adsorption, measurements of relative saturation magnetization, $\Delta M_\infty/M_\infty$, were made at different points during the adsorption process. Results are given in Table 3.

These results confirm that both irreversible and reversible adsorption lead to identical magnetic interaction with the nickel, i.e., the dissociation and electron transfer process is the same. Furthermore, continued decrease in magnetization after 20 h shows that slow uptake still occurs even after establishment of "steady state."

Other workers have discussed the fact that ε is also a function of applied magnetic field (*47*). This was confirmed in Table 4 for fields used in the continuous rate measurements.

By combining the data in Tables 3 and 4 it was possible to calibrate the magnetization change at 14 kOe with amount of hydrogen adsorption using a corrected value of ε. In this way, the continuous rate data shown in Fig. 4 was obtained.

Adsorption was followed at 760 Torr for

TABLE 3

Magnetization Loss on Hydrogen Chemisorption

	Catalyst: 32 wt% Ni/SiO_2 Reduction: 400°C, 4 h R_s: 3.14 nm f_R: 0.707		
P (Torr)	$N_A \times 10^4$ moles/g Ni(red)	$\frac{\Delta M_\infty}{M_\infty}$	ε^a
19.6	12.6	−0.172	−0.70
48.9	13.7	−0.190	−0.71
140.9	14.7	−0.210	−0.73
236.8	15.2	−0.220	−0.74
+20 h	—	−0.250	

[a] $\varepsilon = \frac{\Delta M_\infty}{M_\infty} \frac{(0.606)}{N_A(2)\,(58.9)}$.

TABLE 4

Effect of Applied Field on Magnetization Loss of Adsorption

	Catalyst: 32 wt% Ni/SiO_2 Reduction: 450°C, 16 h R_s: 1.14 nm f_R: 1.00
H (kOe)	$(\Delta M/M)$ 25°C at 760 Torr, 20 h
2.0	−0.482
4.0	−0.462
6.0	−0.450
8.0	−0.435
10.0	−0.423
12.0	−0.413
14.0	−0.407

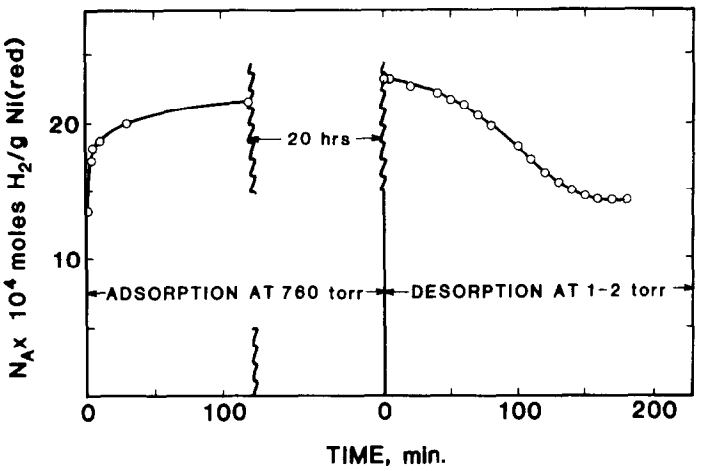

FIG. 4. Time dependence of hydrogen adsorption and desorption (22.9 wt% Ni, R_s = 1.00 nm, f_R = 0.75).

120 min and after a 20-h "soak" period. Desorption at an average hydrogen pressure of 1–2 Torr was then carried out and the rate of removal of adsorbed hydrogen (i.e., gain of magnetization) determined. As anticipated, the initial rate of chemisorption was rapid until irreversible adsorption was complete. The rate continued to decrease by orders of magnitude during subsequent reversible adsorption. Desorption of reversible hydrogen was complete in about 150 min at rates approximately the same as initial reversible uptake. Desorption stopped close to the value of N_0 determined from static volumetric adsorption, validating both experimental procedures and the assumption that extrapolation of the isotherm does indeed give the irreversible amount.

Rates found from the data in Fig. 4 are given in Table 5.

Effect of Unreduced Nickel

Identical magnetic response over the complete chemisorption range rules out any possibility of slow adsorption on unreduced

TABLE 5

Rates of Adsorption and Desorption

Catalyst: 22.9 wt% Ni/SiO_2
Reduction: 450°C, 16 h
R_s: 1.00 nm
f_R: 0.75
N_o: 12.8×10^{-4} mole H_2/g Ni(red)

$N_A \times 10^4$ moles H_2/g Ni(red)	Rate, mole H_2/g Hi(red) min	
	Absorption	Desorption
0–14	1.35×10^{-3}	0
15.5	1.85×10^{-4}	6.50×10^{-6}
17.5	4.50×10^{-5}	9.00×10^{-6}
19.0	7.60×10^{-6}	5.30×10^{-6}
20.5	1.67×10^{-6}	7.50×10^{-6}
23.0	1.67×10^{-7}	2.50×10^{-6}

TABLE 6

Effect of Degree of Reduction

Catalysts: 20–32 wt% Ni/SiO_2
Reduction: 350–450°C, 6–12 h
R_s: 1.14–1.51 nm

Run No.	f_R	R_s (nm)	$N_0 \times 10^4$	$b \times 10^4$	b/N_0
1	0.708	1.16	11.3	0.313	0.0277
2	0.735	1.33	11.3	0.293	0.0259
3	0.781	1.46	12.6	0.298	0.0237
4	0.817	1.34	11.0	0.247	0.0225
5	0.929	1.51	13.9	0.257	0.0185
6	1.00	1.14	10.6	0.183	0.0173

nickel. However, possible influence on the adsorptive properties of metallic nickel through interaction with unreduced phases (SMSI) must be considered. The mechanism is not clear, but could involve electron transfer into surface layers or blockage of metal sites by a layer of unreduced material through which hydrogen must diffuse.

Samples discussed here cover a moderate range of degree of reduction but sufficient to show an effect. Experiments made on a number of similar samples reduced under conditions giving different levels of reduction but with approximately the same crystallite size are shown in Table 6.

Despite the fact that b has a finite value at complete reduction, there is a definite decrease as f_R increases. For example, considering Runs 1 and 6 with crystallite of the same size, a statistical t-test shows a significant difference at the 0.05 level, i.e., there is a 95% probability that the samples are different. Although not a main factor, the presence of unreduced nickel silicate appears to contribute to the slope. These same conclusions apply to the ratio b/N_0. Even the fully reduced catalyst may still contain traces of unreduced material, enough to have an effect.

Effect of Crystallite Size

The effect of crystallite size is seen in a series of sintering experiments on freshly reduced samples. Two types of catalysts are considered, 32–45 wt% Ni/SiO_2 and 6–10 wt% Ni/Al_2O_3. Data are given in Tables 7 and 8, respectively.

For both types of samples, interpretation is complicated by the fact that sintering produces not only an increase of crystallite size but also a major decrease in N_0, reflecting a drop in degree of accessibility or exposure of the surface. Several observations are significant. First, as the crystallite size increases and N_0 decreases, b also decreases but b/N_0 shows an increase. Second, b is a factor of 3–5 greater for the Al_2O_3-supported samples. Finally, there are differences in trends for the samples which may be due to variations in pore size distribution, etc.

It is important to note that sintered states shown in Table 8 indicated no change in

TABLE 7

Effect of Crystallite Size

Catalyst: 25–40 wt% Ni/SiO_2
Reduction: 400°C, 4–8 h
Sintered: 600°C, 4–8 h, He

Sample	f_R	Condition	R_s (nm)	$N_0 \times 10^4$	$b \times 10^4$	b/N_0
25 wt%	0.90	Fresh	1.96	11.1	0.392	.0353
		Sintered	3.36	1.97	0.237	.1203
31 wt%	0.95	Fresh	1.95	13.7	0.352	.0257
		Sintered	2.85	4.03	0.256	.0635
34 wt%	1.00	Fresh	2.04	12.1	0.240	.0198
		Sintered	3.91	3.02	0.200	.0662
36 wt%	0.94	Fresh	2.31	12.3	0.233	.0189
		Sintered	3.05	3.66	0.247	.0674

TABLE 8

Effect of Crystallite Size

Catalyst: 7 wt% Ni/Al_2O_3
Reduction: 400°C, 4–8 h
Sintered: 500–600°C, 1–20 h, He

Sample	f_R	Condition	R_s (nm)	$N_0 \times 10^4$	$b \times 10^4$	b/N_0
1	0.589	Fresh	1.40	7.28	1.48	0.203
		Sintered	1.56	5.17	1.35	0.261
		Sintered	1.73	3.31	1.11	0.335
		Sintered	1.97	2.58	0.833	0.323
		Sintered	2.41	1.34	0.658	0.428
2	0.634	Fresh	1.36	13.8	1.41	0.102
		Sintered	1.62	8.59	1.13	0.159
		Sintered	1.74	7.07	1.06	0.150
		Sintered	2.07	5.04	0.834	0.166
		Sintered	2.28	2.64	0.687	0.260
3	0.645	Fresh	1.53	9.23	1.43	0.154
		Sintered	2.08	4.82	1.33	0.276
		Sintered	2.24	3.35	1.10	0.327
		Sintered	2.68	2.80	0.775	0.277
		Sintered	2.82	1.80	0.697	0.387

saturation magnetization. Increasing the inaccessibility does not appear to involve electronic effects.

Effect of Degree of Accessibility

Possible correlation with degree of accessibility, $\alpha = N_0/N_M$, is best considered by reexamining some of the data in Table 8. Table 9 shows reorganization in which samples have been grouped in three ranges of crystallite size but decreasing values of α.

Within each size group the effect of inaccessibility becomes clear. As the degree of accessibility decreases, the value of b/N_0 increases. The pattern is followed over the size range studied. It is interesting, that for each size, b remains approximately constant but decreases with increasing size. The significance of these results will be discussed later.

Effect of Support

The effect of support material is demonstrated in the data of Fig. 1 and Tables 7 and 8. Yet it should be noted that support is not the only major difference in these samples. Concentration and fractions of reduced nickel are significantly different and complicate direct comparisons.

Nature of Hydrogen Adsorption

In order to clarify the meaning of these results presented above, we summarize the pertinent factors as follows.

(1) There are two types of adsorption—

TABLE 9

Effect of Degree of Accessibility

R_s (nm)	α	$b \times 10^4$	b/N_0
1.36	0.437	1.41	0.102
1.53	0.328	1.43	0.154
1.62	0.324	1.13	0.159
1.40	0.238	1.48	0.203
1.56	0.187	1.35	0.261
2.07	0.242	0.834	0.166
2.08	0.233	1.33	0.276
1.97	0.118	0.833	0.323
2.28	0.140	0.687	0.260
2.41	0.075	0.658	0.428
2.82	0.118	0.697	0.387

Note: Catalyst: same as in Table 8.

very rapid, irreversible adsorption, essentially complete at pressures of 1–2 Torr, with a heat of about 18 kcal/mole, and slow, reversible adsorption that approaches pseudoequilibrium in about an hour but shows continued uptake for 20 h or more, with a heat of adsorption of less than 12 kcal/mole (Fig. 3).

(2) Both types of adsorption are dissociative and donate electrons to the bulk to the same extent (Table 3).

(3) The amount of irreversible adsorption decreases and reversible adsorption increases with temperature (Table 2).

(4) The ratio of reversible to irreversible increases as either the crystallite size increases or the degree of accessibility decreases (Tables 7 and 8).

(5) The ratio of reversible to irreversible varies with the support, increasing from silica to alumina (Tables 7 and 8).

(6) Reversible adsorption decreases as reducibility increases but does not disappear completely at full reduction (Table 6).

Let us examine these observations and their applicability to possibilities outlined earlier. There is little question that irreversible adsorption occurs on exposed centers of high adsorptive energy. Most likely these are on corner and edge sites and atop surface atoms on face planes, as suggested by both experimental evidence on single crystals and theoretical calculations (*31–33*). Low pressure uptake as represented by extrapolation to zero pressure is then a reasonable way to estimate monolayer coverage. The fact that this gives areas smaller than calculated from crystallite size distributions has been interpreted as due to surface inaccessibility (*8*). This conclusion is sensitive to assumptions made in the magnetic calculations, the most critical being shape and a constant stoichiometry of adsorption independent of crystallite size (*9*). Other problems, such as oxygen contamination during measurement, etc. have been thoroughly checked for and ruled out. Shape selection is arbitrary, although most authors favor spherical geometry (*23, 24*). Linsen and Coenen advocate hemispheres (*36*), a model very consistent with strong support bonding, but this would increase α only by a factor of 60%. Trends with values of α less than unity would still exist. Size-dependent considerations are not consistent with observations which show α decreasing with both thermal treatment (*49*) and smaller pore sizes (*37*).

Diffusion to lower energy sites may occur with subsequent replacement from the gas phase. The net result is a further transfer of electrons, with reduced magnetization, and an overall lower heat of adsorption as the hopping-replacement process takes place. Alternatively, reversible adsorption could be direct dissociation on weaker sites. It is impossible to discriminate further on the basis of existing evidence.

There are three possibilities for the location of these weaker sites: (1) lattice positions more appropriately described as "holes" in the surface, i.e., subsurface interstecies, (2) traps deep in the bulk of the crystallite, accessible by diffusion of a permeation or absorption nature, (3) locations within the interface between the metal and the support, i.e., the inaccessible part of the surface.

The key factor is the ratio of b/N_0 and its variation with degree of reduction, crystallite size, degree of accessibility, and support. The factor b is proportional to concentration of sites, $\Sigma_j N_{R_j}$, for an adsorptive process. In the case of diffusion, b is a function of DAt, where D is some diffusion coefficient, A the dimension over which diffusion occurs, and t the time of the process. In either case, N_0 is the exposed nickel surface containing adsorptive sites or from which diffusion must occur.

For adsorption on subsurface positions, b/N_0 is a measure of surface concentration of available sites. Its value should be independent of accessibility for the same crystallite size, degree of reduction and support. Results in Tables 6, 7, 8, and 9 do not indicate this.

With bulk diffusion, N_0 is approximately equivalent to A so that b/N_0 is related to the diffusion coefficient. Likewise, this should be independent of accessibility and degree of reduction. Dependence on crystallite size may be expected since Messner *et al.* (*42*) have calculated that electronegativity differences between nickel and hydrogen decrease for smaller crystallites, thus facilitating adsorption. However, data in Table 9 appear to give the opposite effect. Expected permeation rates are also orders of magnitude lower than those in Table 5 (*41*).

Support effects indicate b/N_0 ratios 4–5 times higher for Al_2O_3 than SiO_2. It could be argued that inclusion of small amounts of aluminum oxide in the nickel might sufficiently alter the interatomic spacings and thus diffusion rates so as to facilitate greater uptake. Similar behavior has been invoked in the concept of paracrystallinity used to explain coprecipitated NiO–Al_2O_3 systems (*52*).

Finally, one must consider that, if subsurface adsorption or diffusion is occurring, then it should be universal. Although reversible adsorption is usually found, there are sufficient and reliable reports of its absence in saturation isotherms (*11*) to suggest that it is some artifact of the catalyst preparation or treatment.

Surface diffusion into the inaccessible interface, on the other hand, is generally more consistent with the data. Table 9 clearly shows an increase in b/N_0 as N_0 decreases, i.e., as the amount of inaccessible surface increases. Tables 7 and 8 support this if the decrease in accessibility is given more importance than the increase in crystallite size. Other supportive evidence includes the increase with the fraction of unreduced nickel compound (Table 6), and the increase for Al_2O_3 (Table 8). It is expected that the chemistry of the support in the interface should play some role. The degree of reduction may be more significant than indicated since Al_2O_3-supported catalysts were poorly reduced.

Our interpretation must be qualitative in the absence of a detailed theory to describe this type of interfacial diffusion. Hydrogen ions are generated on the exposed metal surface and diffuse into the interface in amounts that can be quite large. The nature of the adsorption sites is not apparent. Although not completely conclusive, the weight of evidence favors this model for reversible adsorption. It is hoped that future experiments will be designed to test this hypothesis.

CONCLUSIONS

The reversible mode of adsorption found in hydrogen chemisorption isotherms on nickel has been found to be dissociative, similar to irreversible, but with a lower heat of adsorption. Adsorption on the support or unreduced oxide, spillover to the support and reaction with contamination are ruled out as inconsistent with these properties.

Diffusion into subsurface layers, bulk or inaccessible interface are considered as possibilities. Dependence of the ratio of reversible to irreversible adsorption on factors such as extent of reduction, crystallite size, degrees of accessibility and type of support, as well as measured rates and temperatures dependence, favors the interfacial diffusion model. This explanation is accepted as the most plausible, although many features of the model are not clear.

Determination of the accessible surface area by extrapolation of isotherms to zero pressure is thus the best method for interpreting hydrogen chemisorption measurements.

ACKNOWLEDGMENTS

Some of the data reported here are taken from the results of the following: P. Desai, J. Propp, R. Koveal, Y. Lin, and J. Ginestra. Their contributions to this continuing program are gratefully acknowledged. The authors are also indebted to the Robert A. Welch Foundation who supported much of the work over a period of 10 years, and to the National Science Foundation for additional funding.

REFERENCES

1. Farrauto, R. J., *AIChE Symp. Ser.* **70,** 9 (1974).
2. Hughes, T. R., Houston, R. J., and Sieg, R. P., *Ind. Eng. Chem. Process Des. Dev.* **1,** 96 (1962).

3. Muller, J., *J. Catal.* **6,** 50 (1966).
4. Rostrup-Nielsen, J. P., *J. Catal.* **11,** 220 (1968).
5. Benesi, H. A., Curtis, R. M., and Studer, H. P., *J. Catal.* **10,** 328 (1968).
6. Richardson, J. T., and Freidrich, H., and McGill, R. N., *J. Catal.* **37,** 8 (1968).
7. Richardson, J. T., Crump, J. R., and Osterwalder, R. U., "Sintering and Catalysts." Plenum, New York, 1979.
8. Desai, P. H., and Richardson, J. T., "Catalyst Deactivation." Elsevier, Amsterdam, 1980.
9. Cale, T. S., and Richardson, J. T., *J. Catal.* **79,** 378 (1983).
10. Cale, T. S., and Richardson, J. T., and Ginestra, J., *Appl. Phys. Lett.* **42,** 744 (1983).
11. Barthlolomew, C. H., Pannell, R. B., and Butler, J. L., *J. Catal.* **65,** 335 (1980).
12. Bartholomew, C. H., and Pannell, R. B., *J. Catal.* **65,** 390 (1980).
13. Yates, D., Taylor, W. F., and Sinfelt, J. H., *J. Amer. Chem. Soc.* **86,** 2996 (1964).
14. Kuijpers, E. G. M., Breedijk, A. K., van der Wal, J. J., and Geus, J. W., *J. Catal.* **72,** 210 (1981).
15. Primet, M., Dalman, J. A., and Martin, G. A., *J. Catal.* **46,** 25 (1977).
16. Burch, R., and Flambard, A. R., *J. Catal.* **78,** 389 (1982).
17. Martin, G. A., *J. Catal.* **60,** 345 (1979).
18. Kramer, R., and Andre, M., *J. Catal.* **58,** 287 (1979).
19. Xuan-Zhen, J., Hayden, T. F., and Dumesic, J. A., *J. Catal.* **83,** 168 (1983).
20. Van Meerten, R. Z. C., DeGraat, T. F. M., and Coenen, J. W. E., *J. Catal.* **46,** 1 (1977).
21. Selwood, P. W., "Chemisorption and Magnetization." Academic Press, New York, 1975.
22. Prasad, J., Murthy, K. R., and Menon, P. G., *J. Catal.* **52,** 515 (1978).
23. Hardeveld, R., and Hartog, F., *Surf. Sci.* **15,** 189 (1969).
24. Hardeveld, R., and Hartog, F., "Advances in Catalysis," Vol. 43, p. 86. Academic Press, New York, 1972.
25. Balkely, D. W., and Somorjai, G. A., *J. Catal.* **42,** 181 (1976).
26. Bond, G. C., *Discuss. Faraday Soc.* **41,** 200 (1966).
27. Shopov, D., Andreev, A., and Petkov, D., *J. Catal.* **13,** 123 (1969).
28. Fassaert, D. J. M., and van der Avoird, A., *Surf. Sci.* **55,** 291 (1976).
29. Sweet, F., and Rideal, E., "Actes du Deuxieme Congre International de Catalyse." Technip, Paris, 1961.
30. Fassaert, F. J. M., and van der Avoird, A., *Surf. Sci.* **55,** 313 (1976).
31. Christmann, K., *Bull. Soc. Chim. Belg.* **88,** 519 (1979).
32. Lapeyoulade, J., and Neil, K. S., *J. Chem. Phys.* **70,** 789 (1973).
33. Slinken, A. A., Kucherov, A. V., and Rubinshlein, A. M., *Kinet. Catal.* **19,** 415 (1978).
34. Konvalinka, J. A., Van Oeffelt, P. H., and Scholten, J. J., *Appl. Catal.* **1,** 141 (1981).
35. Bond, G. C., "Catalysis by Metals." Academic Press, New York, 1962.
36. Linsen, B. G., and Coenen, J. W. E., "Physical and Chemical Aspects of Adsorbents and Catalysts." Academic Press, New York, 1970.
37. Richardson, J. T., and Propp, J. L., *J. Catal.* **98,** 457 (1986).
38. Tauster, S. J., Fung, S. C., and Garteu, R. L., *J. Amer. Chem. Soc.* **100,** 170 (1978).
39. Martin, G. A., and Dalmon, J. A., *React. Kinet. Catal. Lett.* **16,** 325 (1981).
40. Magcelin, G., and Lester, J. E., *J. Catal.* **93,** 270 (1985).
41. McLellan, R. B., and Harkins, C. G., *Mater. Sci.* **18,** 5 (1975).
42. Messmer, R. P., Salahub, D. R., Johnson, K. H., and Yang, C. Y., *Chem. Phys. Lett.* **51,** 84 (1977).
43. Nagy, F., Moger, D., Hegedus, M., Mink, G., and Szabo, S., *Acta. Chim. Acad. Sci. Hong.* **100,** 211 (1979).
44. Menon, P. G., and Froment, G. F., *Appl. Catal.* **1,** 31 (1981).
45. Den Otter, G. J., and Dautzenberg, F. M., *J. Catal.* **51,** 26 (1978).
46. Knor, Z., *in* "Catalysis, Science and Technology," Vol. 3 (J. R. Anderson and M. Boudart, Eds.). Springer-Verlag, New York, 1982.
47. Martin, G. A., DeMontgolfier, P., and Imelik, B., *Surf. Sci.* **36,** 675 (1973).
48. Ginestra, J. M. R., "Magnetic Study of Small Silica-Supported Nickel Clusters," Ph.D. dissertation. Dept. Chem. Eng., Univ. of Houston, August, 1983.
49. Richardson, J. T., and Koveal, R., *J. Catal.* **98,** 559 (1986).
50. Propp, J. L., "Support Pore Effects in Sintering on Nickel Catalysts," M.S. thesis. Dept. Eng., Univ. of Houston, April, 1981.
51. Richardson, J. T., and Dubus, R. J., *J. Catal.* **54,** 207 (1978).
52. Puxley, D. C., "Preparation of Catalysts III." Elsevier, Amsterdam, 1983.